INTERNATIONAL JOURNAL FOR NUMERICAL METHODS IN FLUIDS
Int. J. Numer. Meth. Fluids 2004; **46**:1049–1067
Published online 27 September 2004 in Wiley InterScience (www.interscience.wiley.com). DOI: 10.1002/fld.789

Development of a generalized multi-layer model for 3-D simulation of free surface flows

A. R. Zarrati[1,*,†] and Y. C. Jin[2,‡]

[1]*Department of Civil Engineering, Amirkabir University of Technology, No. 424, Hafez Avenue, Tehran 15914, Iran*
[2]*Faculty of Engineering, University of Regina, Regina, SK, Canada S4S 0A2*

SUMMARY

A mathematical model was developed for three-dimensional (3-D) simulation of free surface flows. In this model, the flow depth is divided into a number of layers and shallow water equations are integrated in each layer to derive the hydrodynamic equations. To give a general form to this model, each layer is assumed to be non-horizontal with varying thickness in the flow domain. A non-orthogonal curvilinear coordinate system is employed in the model, to allow for flexibility in dealing with the irregular geometry of natural watercourses.

Due to the similarity in governing equations, two-dimensional (2-D) depth averaged programs can be developed into a multi-layer model. The development for a depth averaged program and its numerical scheme is described in this paper.

Experimental data and semi-analytical solutions are used to evaluate the performance of the model. Three different cases of open channel flow are tested: 1-flow in a straight open channel, 2-the flow development region in a channel, and 3-flow in a meandering channel. It is shown that the model has the capability to predict velocity distribution and secondary flows in complex 3-D flow conditions.

KEY WORDS: multi-layer model; shallow water equations; 3-D model; free surface; curvilinear co-ordinates; secondary flow; meandering channel

INTRODUCTION

Prediction of the flow pattern and the characteristics of fluid flow in rivers and open channels has been the subject of research for many years. Three-dimensional mathematical models are necessary to compute the water surface elevation and the velocity distribution in three principle directions by solving the Navier–Stokes equations. Irregularity in the flow boundaries increases the complexity of these problems. Generally, the width and the length of the river or channel

*Correspondence to: A. R. Zarrati, Department of Civil Engineering, Amirkabir University of Technology, No. 424, Hafez Avenue, Tehran 15914, Iran.
†E-mail: zarrati@aut.ac.ir
‡E-mail: jiny@uregina.ca

Contract/grant sponsor: National Science and Engineering Research Council of Canada

Received 9 September 2003
Revised 19 June 2004

are much larger than the depth. Therefore, the depth-wise component of the fluid motion is much weaker than the fluid motion in the other two directions. This assumption leads to a great simplicity in the governing equations of fluid motion and reduces the momentum equation in the depth-wise direction to the simple hydrostatic law [1]. The result of the simplification yields the equations referred to as the 3-D shallow water equations.

When the shallow water equations are integrated over the whole flow depth of the channel, the 2-D depth averaged equations are obtained. Many mathematical models have been developed based on 2-D depth averaged equations including those developed by Vreugdenhil and Wijbenga [2], Molls and Chaudhry [3], Jin and Steffler [4], and Ye and McCorquodale [5]. While these models allow for the water surface profile to be calculated without any additional relationship, a full 3-D model requires knowledge of kinematic and dynamic boundary conditions and makes use of more sophisticated computations to determine the free surface profile. Depth averaged models provide satisfactory results for many practical purposes. However, they give no information on longitudinal velocity and secondary flow distribution in depth. In addition, the effective stresses resulting from the depth integration of the non-linear convective accelerations (momentum dispersion) are usually neglected in these models, which causes a certain degree of inaccuracy [1].

In order to take advantage of the shallow water equations while avoiding the drawbacks of 2-D depth averaged models, a multi-layer system was adopted in this study. In this system, the water column is divided into a number of layers that share friction terms and convective fluxes. There has been a number of research works on multi-layer models. These works have primarily been done in coastal zones, under the assumption that the flow can be viewed as horizontal layers with the thickness of each layer constant throughout the flow domain [6–10]. A few researchers have also applied the multi-layer system in open channels with the same assumption of horizontal layers of constant thickness [11–13]. This assumption causes some restriction in channel flows and since the top layer must accommodate all of the water surface variation, it may become too thick for the model accuracy in different locations. An additional complication occurs when the lower layers of flow intersect the bed topography and the imposing boundary conditions become very complex.

In the present work, at the first stage, formulation of a generalized multi-layer model is derived. In this model, each layer is assumed to be non-horizontal with varying thickness in the flow domain. A non-orthogonal curvilinear system is also employed to allow for flexibility in dealing with irregularities in the flow boundaries. The development of a multi-layer model using a 2-D depth averaged model is discussed followed by a discussion of the extension of the finite volume scheme used in the 2-D model to solve the multi-layer system. The model is tested for three different cases of open channel flow: (1) a M2 profile in a long channel, (2) flow development region in a rectangular channel, and (3) flow in a meandering channel. These tests demonstrate the ability of the model to calculate the velocity distribution in depth and secondary flows in channel bends.

GOVERNING EQUATIONS

A multi-layer model is based on the computation of momentum and mass fluxes in different layers of the system (Figure 1). Integration of the equations in each layer can be applied to obtain a relationship for the average velocities within that layer. The derived equations are

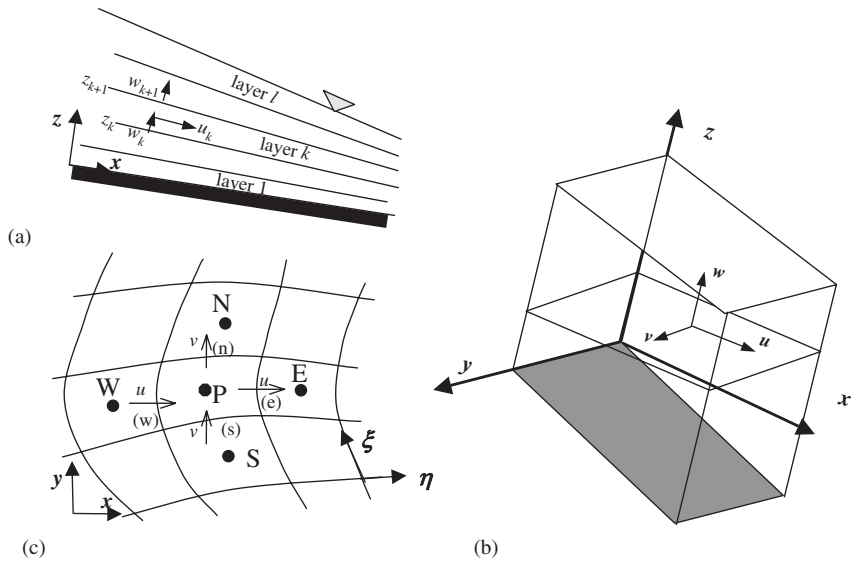

Figure 1. Layout of multi-layer system and location of variables.

similar to depth averaged equations with additional terms for the transfer of momentum and mass flux between the layers. This process results in converting a 3-D problem into a number of 2-D problems.

The 3-D shallow water equations for steady-state conditions, neglecting wind stresses and coriolis effects, in the Cartesian co-ordinate system are:

$$\frac{\partial u}{\partial x}+\frac{\partial v}{\partial y}+\frac{\partial w}{\partial z}=0 \tag{1}$$

$$\frac{\partial(uu)}{\partial x}+\frac{\partial(uv)}{\partial y}+\frac{\partial(uw)}{\partial z}=-\frac{1}{\rho}\frac{\partial p}{\partial x}-g_x+\frac{\partial}{\partial x}\left(\upsilon_t\frac{\partial u}{\partial x}\right)+\frac{\partial}{\partial y}\left(\upsilon_t\frac{\partial u}{\partial y}\right)+\frac{\partial}{\partial z}\left(\upsilon_t\frac{\partial u}{\partial z}\right) \tag{2}$$

$$\frac{\partial(vu)}{\partial x}+\frac{\partial(vv)}{\partial y}+\frac{\partial(vw)}{\partial z}=-\frac{1}{\rho}\frac{\partial p}{\partial y}-g_y+\frac{\partial}{\partial x}\left(\upsilon_t\frac{\partial v}{\partial x}\right)+\frac{\partial}{\partial y}\left(\upsilon_t\frac{\partial v}{\partial y}\right)+\frac{\partial}{\partial z}\left(\upsilon_t\frac{\partial v}{\partial z}\right) \tag{3}$$

$$\frac{\partial p}{\partial z}=-\rho g_z \tag{4}$$

where u, v and w are velocity components in the x, y and z (depth) directions, respectively; p is pressure; ρ is density; g_x, g_y and g_z are components of gravitational acceleration in each of the three directions; and υ_t is eddy viscosity. Density is assumed to be constant in these equations. Equation (4) is first substituted into Equations (2) and (3). The resulting equations are then integrated over the kth layer assuming a control volume with upper and lower surfaces inclined in both the x and y directions (Figure 1(b)). In this integration, Leibnitz rule is used:

$$\int_{z_k}^{z_{k+1}}\frac{\partial f}{\partial k}\,\mathrm{d}z=\frac{\partial}{\partial k}\int_{z_k}^{z_{k+1}}f\,\mathrm{d}z+f\left.\frac{\partial z}{\partial k}\right|_{z_k}-f\left.\frac{\partial z}{\partial k}\right|_{z_{k+1}} \tag{5}$$

where z_k and z_{k+1} denote the co-ordinates of the bottom and top surfaces of a layer along the z axis. Following the process of integration, the governing equations become

$$\frac{\partial(U h_k)}{\partial x} + \frac{\partial(V h_k)}{\partial y} + M|_{z_k} - M|_{z_{k+1}} = 0 \tag{6}$$

where

$$M = u\frac{\partial z}{\partial x} + v\frac{\partial z}{\partial y} - w \tag{7}$$

$$\frac{\partial(UU h_k)}{\partial x} + \frac{\partial(UV h_k)}{\partial y} = -g h_k \frac{\partial \zeta}{\partial x} + \frac{\partial}{\partial x}\left[\upsilon_t \frac{\partial(U h_k)}{\partial x}\right] + \frac{\partial}{\partial y}\left[\upsilon_t \frac{\partial(U h_k)}{\partial y}\right] + \mathrm{Sr}^u|_{z_k} - \mathrm{Sr}^u|_{z_{k+1}} \tag{8}$$

$$\mathrm{Sr}^u = \nu_t\left(2\frac{\partial u}{\partial x}\frac{\partial z}{\partial x} + 2\frac{\partial u}{\partial y}\frac{\partial z}{\partial y} - \frac{\partial u}{\partial z}\right) - M \cdot u \tag{9}$$

$$\frac{\partial(VU h_k)}{\partial x} + \frac{\partial(VV h_k)}{\partial y} = -g h_k \frac{\partial \zeta}{\partial y} + \frac{\partial}{\partial x}\left[\upsilon_t \frac{\partial(V h_k)}{\partial x}\right] + \frac{\partial}{\partial y}\left[\upsilon_t \frac{\partial(V h_k)}{\partial y}\right] + \mathrm{Sr}^v|_{z_k} - \mathrm{Sr}^v|_{z_{k+1}} \tag{10}$$

$$\mathrm{Sr}^v = \nu_t\left(2\frac{\partial v}{\partial x}\frac{\partial z}{\partial x} + 2\frac{\partial v}{\partial y}\frac{\partial z}{\partial y} - \frac{\partial v}{\partial z}\right) - M \cdot v \tag{11}$$

where h_k is the layer thickness; ζ is water surface elevation; $\partial z/\partial x$ and $\partial z/\partial y$ are the slopes of the layer interfaces in the x and y directions; and U and V are average velocities in the center portion of each layer as

$$U = \frac{1}{h_k}\int_{z_k}^{z_{k+1}} u\,\mathrm{d}z, \quad V = \frac{1}{h_k}\int_{z_k}^{z_{k+1}} v\,\mathrm{d}z \tag{12}$$

The term M is the mass flux across the layer interfaces and is zero for the upper interface of the top layer (water surface) and the lower interface of the bottom layer (channel bed). In the sources of the momentum equations (Equations (9) and (11)), the terms in the brackets show shear stresses on the interfaces. Shear stresses on the water surface are zero, when wind stress is neglected. Shear stresses on the lower interface of the bottom layer are due to bed friction. Second terms in the source that is Mu and Mv are convective fluxes due to mass transfer between the layers.

As mentioned previously, neglecting momentum dispersion terms causes some inaccuracy in 2-D depth averaged models. However, in a multi-layer model, when the flow depth is divided into a sufficient number of layers, velocities are nearly uniform in every layer. As a result, momentum dispersion terms are small and they are therefore neglected in this model.

To deal with the complexity of the river geometry, a non-orthogonal curvilinear system (boundary fitted coordinates) is employed in the x and y directions (Figure 1(c)). Cartesian velocity components are selected as the dependent variables, to avoid curvature sensitive terms (Christoffel symbols). In this model, a mixture of Contravariant and Cartesian velocity components are used to keep the equations in a more compact form. Transformed governing equations are given in Appendix A. In this way the model has the flexibility of working with curved boundaries in the flow direction. On the other hand, formulation of the model for non-parallel layers with thickness of each layer varying, makes it possible to easily locate any number of layers in the flow domain. In the model, a higher resolution of layers can be achieved, either by increasing the number of layers, or by reducing the thickness of layers near the bed or at any specified water depth.

SOLUTION ALGORITHM AND THE NUMERICAL SCHEME

To discretize the governing equations, they were integrated over the cells in each layer according to the finite volume method and solved in an iterative manner. To avoid so-called checkerboard, non-physical, pressure oscillation and excessive interpolations, a staggered grid was employed [14]. Solution of the discretized momentum equations in each layer, considering boundary conditions, yields the layer averaged velocity components in the x and y directions at all grid points. These velocities may not satisfy the continuity equation as they are based on flow depth and velocities from the previous iteration and therefore need to be corrected [12, 15, 16]. For coupling depth and velocity fields, an equation for depth correction was also derived by using momentum and continuity equations.

After discretization, the momentum equation for U in a specific layer is written as

$$a_p^U U_p = \sum_{nb=E,W,N,S} a_{nb}^U U_{nb} + \mathrm{Sr}^U - gh_k\left(y_\eta \frac{\partial \zeta}{\partial \xi} - y_\xi \frac{\partial \zeta}{\partial \eta}\right)\Delta\eta\Delta\xi \tag{13}$$

where a is a coefficient of the discretized equation; P, E, W, N and S denote a grid point and four points surrounding it; superscript U specifies the momentum equation for U; Sr^U is the source term which includes all of the terms given in S^φ and S_c^φ of Equation (A2) except the gravity terms; and $\Delta\eta$ and $\Delta\xi$ are the dimensions of the mesh in the computational domain. When an asterisk sign is used to show the value of the velocity components and depth in the process of iteration:

$$U = U^* + U', \quad V = V^* + V' \quad \text{and} \quad H = H^* + H' \tag{14}$$

where prime ($'$) shows the correction required to obtain the correct values and H is the total depth. The thickness of all layers except for the top one is fixed and does not change in the calculation procedure. In the process of iteration, Equation (13) is written as

$$a_p^U U_p^* = \sum_{nb=E,W,N,S} a_{nb}^U U_{nb}^* + \mathrm{Sr}^U - gh_k\left(y_\eta \frac{\partial \zeta^*}{\partial \xi} - y_\xi \frac{\partial \zeta^*}{\partial \eta}\right)\Delta\eta\Delta\xi \tag{15}$$

Subtracting Equation (15) from Equation (13) results in

$$a_p^U U_p' = \sum_{nb=E,W,N,S} a_{nb}^U U_{nb}' - gh_k\left(y_\eta \frac{\partial H'}{\partial \xi} - y_\xi \frac{\partial H'}{\partial \eta}\right)\Delta\eta\Delta\xi \tag{16}$$

Following the SIMPLEC algorithm [14]:

$$U_p = U_p^* - gh_k\left(y_\eta \frac{\partial H'}{\partial \xi} - y_\xi \frac{\partial H'}{\partial \eta}\right)\Delta\eta\Delta\xi/C_{\mathrm{ef}U} \tag{17}$$

Similarly for V velocity:

$$V_p = V_p^* - gh_k\left(x_\xi \frac{\partial H'}{\partial \eta} - x_\eta \frac{\partial H'}{\partial \xi}\right)\Delta\eta\Delta\xi/C_{\mathrm{ef}V} \tag{18}$$

where $C_{\mathrm{ef}U} = a_P^U - \Sigma a_{nb}^U$ and $C_{\mathrm{ef}V} = a_P^V - \Sigma a_{nb}^V$. The continuity equation for the whole flow depth can be written as

$$\sum_{k=1}^{k=\mathrm{nl}} \frac{\partial(U_c h_k)}{\partial \xi} + \sum_{k=1}^{k=\mathrm{nl}} \frac{\partial(V_c h_k)}{\partial \eta} = 0 \tag{19}$$

where nl is the number of layers. Substituting Equations (17) and (18) into the discretized continuity equation results in an equation for depth correction. However, this equation contains more than five unknown points of H' as is the case in a Cartesian co-ordinate system and therefore, it is not suitable for an efficient tri-diagonal solver (TDMA). Since depth corrections approach zero in the process of iteration, the second terms in Equations (17) and (18) that is, $y_\xi\,\partial H'/\partial\eta$ and, $x_\eta\,\partial H'/\partial\xi$, may be neglected without affecting the accuracy of results for velocity and water depth. It was also reported that in closed conduit computation, keeping these terms did not help the speed of convergence [17]. The final form of the depth correction equation takes the following form:

$$a_P H'_P = a_E H'_E + a_W H'_W + a_N H'_N + a_S H'_S + \mathrm{Su} \tag{20}$$

where Su is the difference between the outflow and inflow of each water column and is called mass residual. At the converged solution, Su should become zero and the sum of absolute value of Su over all the columns normally serves as an indicator of the convergence during the solution. In addition:

$$a_E = -g\Delta\eta^2 \sum_{k=1}^{k=\mathrm{nl}} \left[h_k^2\left(\frac{y_\eta^2}{C_{\mathrm{ef}U}} + \frac{x_\eta^2}{C_{\mathrm{ef}V}}\right)\right]_e; \quad a_W = -g\Delta\eta^2 \sum_{k=1}^{k=\mathrm{nl}} \left[h_k^2\left(\frac{y_\eta^2}{C_{\mathrm{ef}U}} + \frac{x_\eta^2}{C_{\mathrm{ef}V}}\right)\right]_w$$

$$a_N = -g\Delta\xi^2 \sum_{k=1}^{k=\mathrm{nl}} \left[h_k^2\left(\frac{y_\xi^2}{C_{\mathrm{ef}U}} + \frac{x_\xi^2}{C_{\mathrm{ef}V}}\right)\right]_n; \quad a_S = -g\Delta\xi^2 \sum_{k=1}^{k=\mathrm{nl}} \left[h_k^2\left(\frac{y_\xi^2}{C_{\mathrm{ef}U}} + \frac{x_\xi^2}{C_{\mathrm{ef}V}}\right)\right]_s$$

and

$$a_p = a_E + a_W + a_N + a_S \tag{21}$$

As illustrated in Figure 1, c, e, w, n and s are positions at the face of the scalar cells.

Therefore, the solution algorithm can be summarized as follows:

1. Initial and boundary conditions for all values are set.
2. Momentum equations for U and V (Equation (A2)) are solved for all layers to find U and V at all grid points in the 3-D space.
3. The depth correction equation (Equation (20)) is solved and flow depth is updated.

4. Velocities are updated based on the depth correction values to satisfy continuity using Equations (17) and (18).
5. Velocity components in the depth direction, w, defined at the interfaces of the layers are calculated from the continuity equation in each layer (Equation (A1)) starting from the bottom layer.
6. Criteria for convergence is checked and if it is not satisfied, calculation steps two to six are repeated.

To set the initial water depth and layout of the layers, it is advantageous to run the program first with one layer (that is a 2-D depth-average model) and estimate the location of the water surface. The accuracy of water surface, calculated from the 2-D depth averaged model, depends on the assumed friction coefficient and the importance of the momentum dispersion terms (which are usually neglected in 2-D models). The resulting flow depth can then be divided into any number of layers, with refinement of layers at any specified water depth, for use in the multi-layer model.

In sub-critical flows studied here, the flow depth is specified at the outlet section. At the inlet, the depth gradient is set to zero. No boundary condition is necessary for U velocities at the outlet [14] and $\partial V/\partial x = 0$. The velocity distribution at the inlet is calculated in each iteration using the values of the discharge and the depth. Depending on the problem, an appropriate distribution law (for example logarithmic distribution) should be assumed for velocity at inlet. At the side walls and channel bed, velocities normal to the wall are set to zero. Also, the wall function [18] is employed to link the velocities at the first grid point or in the bottom layer to boundary shear stresses. The depth correction at all boundaries is set to zero.

UPGRADING A 2-D DEPTH AVERAGED MODEL TO A 3-D MULTI-LAYER MODEL

A multi-layer model is in fact the solution of layer averaged momentum equations (which are similar to depth averaged equations) in a number of layers. One of the advantages of a multi-layer system is that due to this similarity, a 3-D multi-layer model can be developed from any 2-D depth-averaged program. To upgrade any depth averaged model, additional terms should be added to the momentum equations to account for friction and mass transfer between the layers. The momentum equations should be solved in a similar manner for each layer. Following this step, the flow depth should be updated and the iteration process continues until convergence is achieved. In the finite volume scheme, the discretized momentum equation for a 2-D depth averaged model is

$$a_p \varphi_p = a_E \varphi_E + a_W \varphi_W + a_N \varphi_N + a_S \varphi_S + \text{Source} \tag{22}$$

where

$$a_p = \sum_{nb=E,W,N,S} a_{nb} + F_E - F_W + F_N - F_S \tag{23}$$

and the F terms are the mass fluxes in and out of a cell face. In a 2-D model, the sum of the mass fluxes in and out of a cell face is zero. When a 2-D model is upgraded to a 3-D

multi-layer model, the sum of the F terms is not zero. Instead, the sum is

$$F_E - F_W + F_N - F_S = M|_{z_k} - M|_{z_{k+1}} \tag{24}$$

Since the sum of the F terms may be positive or negative, it cannot be added to the right hand side of Equation (23). If the sum is negative, a_p will become smaller than the sum of the neighbouring coefficients, $\sum a_{nb}$, and this does not comply with the main rules of obtaining a converged solution [14]. A simple solution to this problem is to multiply this sum by φ_p, and add the resulting term to the 'source' term, on the other side of the equation.

MODEL VERIFICATION

The following section describes the ability of the model to calculate velocity distribution in depth and secondary flows for three cases of open channel flow.

Case 1: water surface and velocity distribution for a M2 profile

The purpose of this test was to check the ability of the model to predict water surface and velocity profiles where a semi-analytical equation can be derived for velocity distribution in depth. A 3 m wide, 20 m long channel with 0.0005 slope and 1.2 m^3/s discharge was considered. Absolute roughness of the channel bed, k_s, was assumed to be 0.15 m. Tail water was fixed at 0.26 m, which is close to the critical flow depth. The water surface profile was calculated using the direct step method [19]. To calculate the energy slope, the effect of flow depth on the roughness coefficient was also considered. A logarithmic distribution was found for the velocity, by assuming that the mixing length was equal to κz, where κ is the Von Karman constant and z is the distance measured from the bed. The distribution of shear stress was assumed to be linear from a maximum value at the channel bed to zero at the surface. Following the Parandl's approach [20], the following equation was derived:

$$\frac{u}{u_*} = \frac{2}{\kappa}\left(\sqrt{1-\frac{z}{H}} - \ln\frac{1+\sqrt{1-z/H}}{\sqrt{z/H}}\right) + C \tag{25}$$

where u_* is the bed shear velocity and C is the constant of integration. Near the bed, where the shear stress is almost equal to the bed shear stress, the velocity distribution for a rough bed can be written as

$$\frac{u}{u_*} = \frac{1}{\kappa}\ln\left(\frac{30z}{k_s}\right) \tag{26}$$

For small values of z/H, Equations (25) and (26) should give the same value for velocity and therefore

$$C = \frac{1}{\kappa}\ln\left(\frac{16.25H}{k_s}\right) \tag{27}$$

From the velocity distribution, a relationship can be derived for discharge. When the discharge is known, u_* can be calculated at any section.

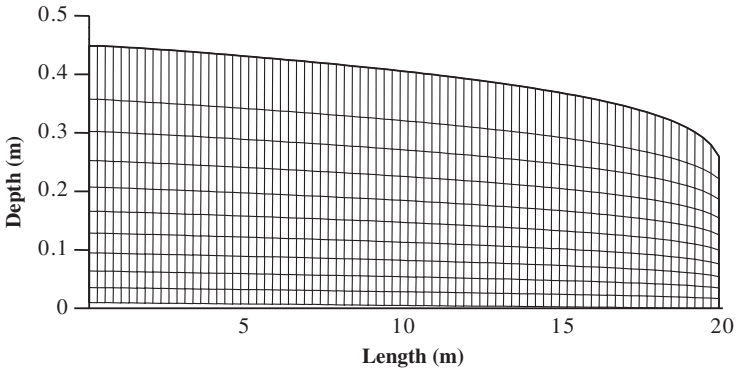

Figure 2. Arrangement of layers for calculation of water surface and velocity profiles along a M2 profile.

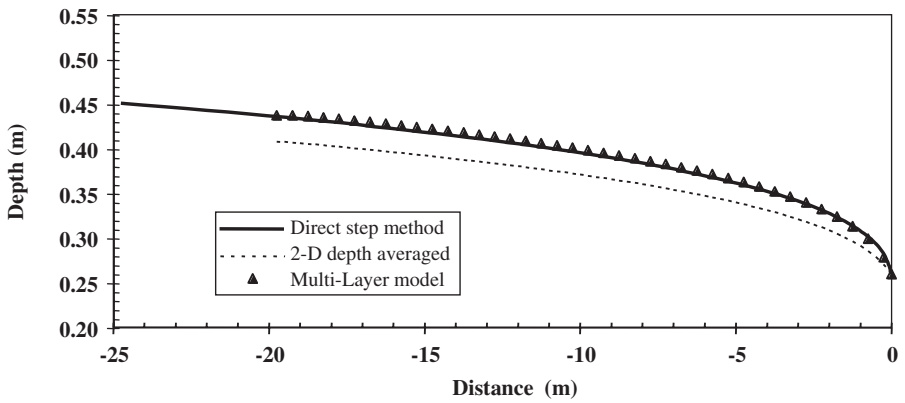

Figure 3. Comparison of calculated water surface profile with direct step method.

The model was first executed with one layer representing the whole flow depth, and the estimated water surface was used as the initial value for the multi-layer model. In the one-layer calculations, the bed friction was estimated based on Manning's equation with a constant value of 0.03 as Manning's roughness coefficient. This value was determined from the bed absolute roughness under uniform flow condition. The model was then executed with 10 layers. The thickness of the layers was decreased by 10% towards the bed. This allowed for a better resolution near the channel bed, where velocity gradients are high (Figure 2). Eddy viscosity was calculated at the interfaces of the layers from mixing length similar to that used in deriving Equation (25).

The water surface profile calculated by the multi-layer model, conforms well with that determined from the direct step method (Figure 3). Figure 4 shows the velocity profiles at two sections, one close to the inlet and one close to the outlet. These profiles illustrate good agreement with the logarithmic velocity distribution (Equation (25)).

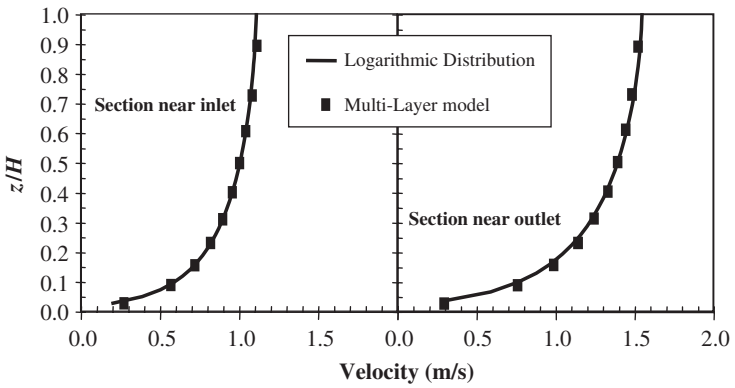

Figure 4. Comparison of calculated velocity profiles with logarithmic distribution.

It should be noticed that if parallel layers were used in this problem, the top layer thickness would have increased to approximately 8 times the thickness of the layer below it at the inlet.

Case 2: developing region in a rectangular channel

Ranga Raju *et al.* [21] studied the developing regions in open channels. Knowing that at the inlet velocity distribution is uniform over the entire depth, the length of the developing region was defined as a length, where flow parameters such as the flow velocity at water surface, U_e attained 99% of their final value. Ranga Raju *et al.* [21] measured velocity profiles along the centerline of a 75 cm wide flume at different distances from the inlet. They showed that the dimensionless length (L/H) of the flow-developing region is a function of the flow aspect ratio (H/B) and the channel roughness, where B is the channel width.

Flow in a developing region is complex, three-dimensional, and influenced by secondary circulation and free surface effects. One of the tests was simulated using the multi-layer model with the entrance velocity equal to 0.3 m/s and smooth boundaries (Run 8). 14 m of the channel length was modelled and satisfactory results were obtained using a 100×15 mesh in the flow direction and 10 layers in depth. The thickness of the layers was reduced by 25% towards the bed to obtain a better resolution in the zone with higher gradients of velocity. Mixing length distribution in depth, as suggested by Nezu and Rodi [22] for fully developed flows in straight rectangular channels, was used to calculate eddy viscosity. A uniform velocity distribution was set at the channel inlet. Velocity profiles at different sections in the developing zone were calculated and compared with experimental data (Figure 5). There appears to be a good agreement between the data sets despite the simple turbulence model used here. The surface velocity variation along the developing zone was also compared with experimental measurements. Figure 6 shows the good agreement between the two sets of data. The velocity profile calculated at a section 11 m downstream of the inlet without the effect of side wall friction is also plotted in Figure 5. When this profile is compared with the profile that includes the effect of wall friction, it is shown how boundary layer development at the two side walls creates a flow towards the channel centerline and increase the velocity at the mid section of the channel. This effect is well simulated by the multi-layer model.

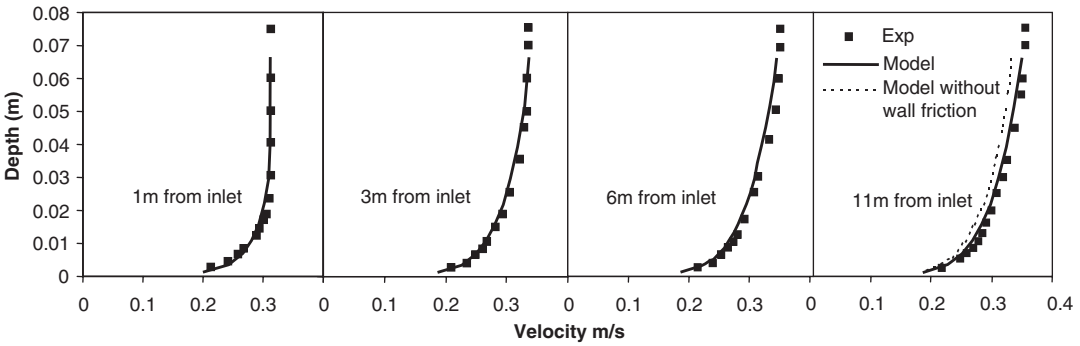

Figure 5. Comparison of calculated velocity profiles along the developing zone with experimental data.

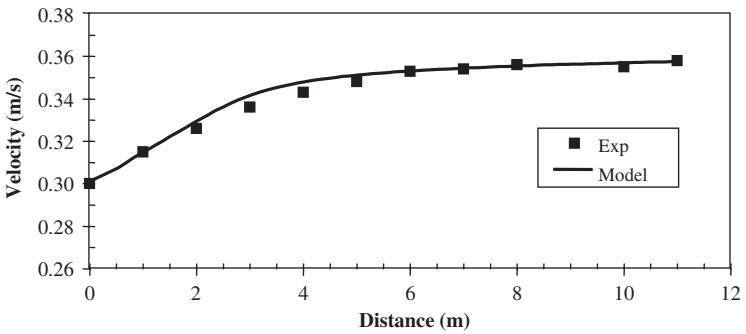

Figure 6. Comparison of surface velocity along the developing zone with experimental data.

Case 3: meandering channel with 90° *bends*

The ability of the model to predict secondary flows was tested by simulating flow in a meandering channel. Tamai *et al.* [23] studied flow characteristics in a meandering channel. The experimental channel consisted of 10 consecutive bends with a rectangular cross section. The radius of the channel centerline was 0.6 m with 90° bends. Each bend was connected to the next with a straight reach 0.3 m long, and 0.3 m wide. The channel bed and walls were reported to be hydraulically smooth and the longitudinal channel slope was 0.001. Flow discharge was $0.002\ m^3/s$.

Tamai *et al.* [23] concluded that at the beginning of a bend, the secondary current developed in a preceding bend occupies the whole section. Further into the bend, the secondary current produced in the present bend begins to develop near the bed. In the mid section of the bend, two opposing, circulating secondary currents coexist. In the exit region, a new secondary current finally occupies the whole section. The secondary flow pattern in a meandering channel is therefore quite complicated as the growth of a spiral flow in a bend is strongly affected by the residual spiral from the preceding bend.

To simulate the secondary flows, four consecutive bends were modelled using 160×10 mesh and 8 layers of equal thickness. With this number of mesh and layers, the results were

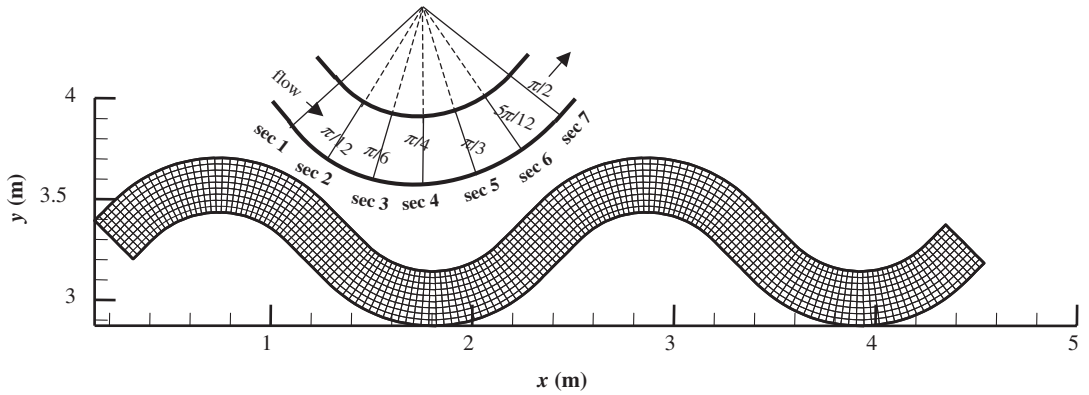

Figure 7. Layout of the meandering channel and measurement sections.

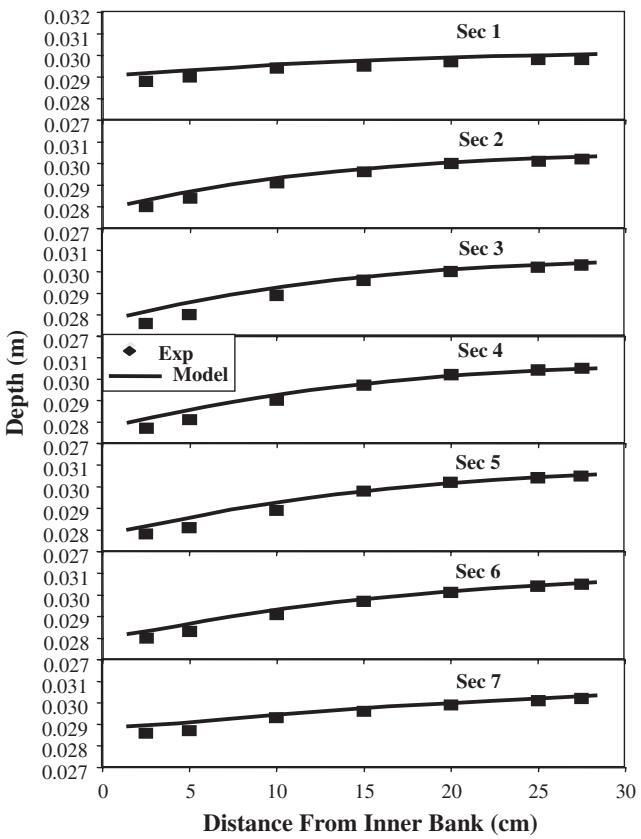

Figure 8. Water surface profiles along the bend.

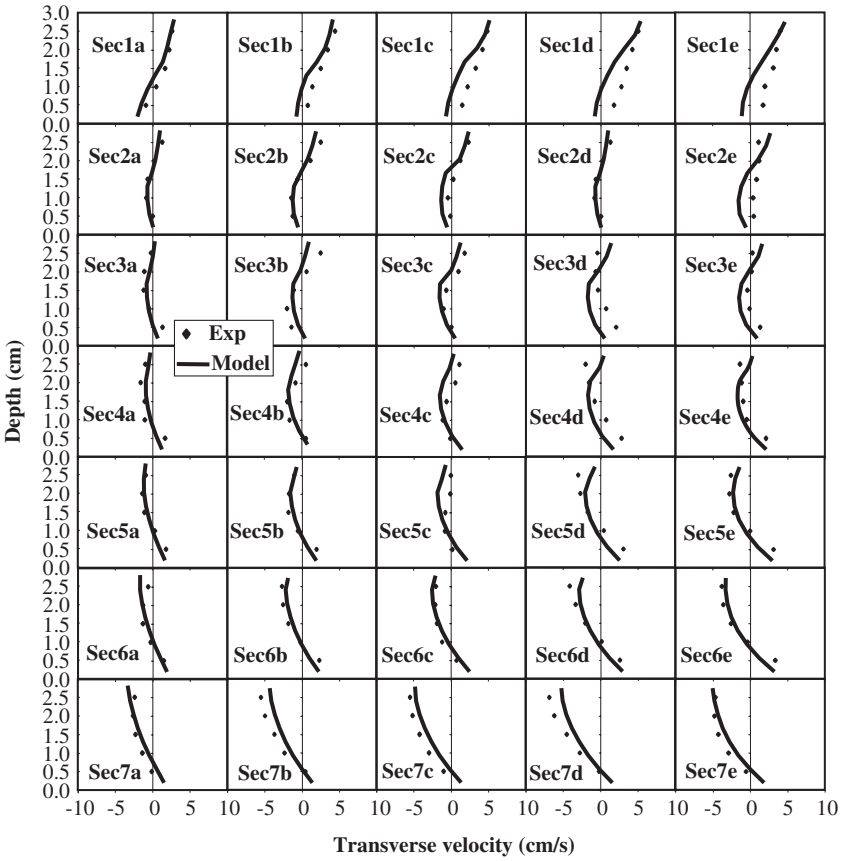

Figure 9. Transverse velocity profiles in different locations along the bend.

found to be independent of mesh size and number of layers. The same simple mixing length model that was used in Case 2 was also employed for the third study case. Layout of the computational domain and the position of seven measurement sections are shown in Figure 7. These seven sections are located at 15° intervals across the bend. Calculated water surface profiles at these seven sections were compared with experimental measurements as shown in Figure 8. The maximum difference between the calculated depth and measurements was 1.4% over estimation of the depth at the lowest measured water surface position along the bend in Section 3. Transverse and longitudinal velocity profiles at the sections along the bend and in each section at five different locations, denoted by *a* to *e*, are also compared with experimental data in Figures 9 and 10. From these locations, *c* is at the centerline and the other sections are at 10 cm intervals on the right and left hand side of the centerline, with location *a* near the outer bank. In Figure 9, negative transverse velocity indicates that the flow is towards the outer bank. Despite the complex flow pattern and the use of a simple turbulence model, the agreement between the calculated and experimental data is good. Employing a more advanced turbulence model will improve the results. The decay of the spiral flow coming

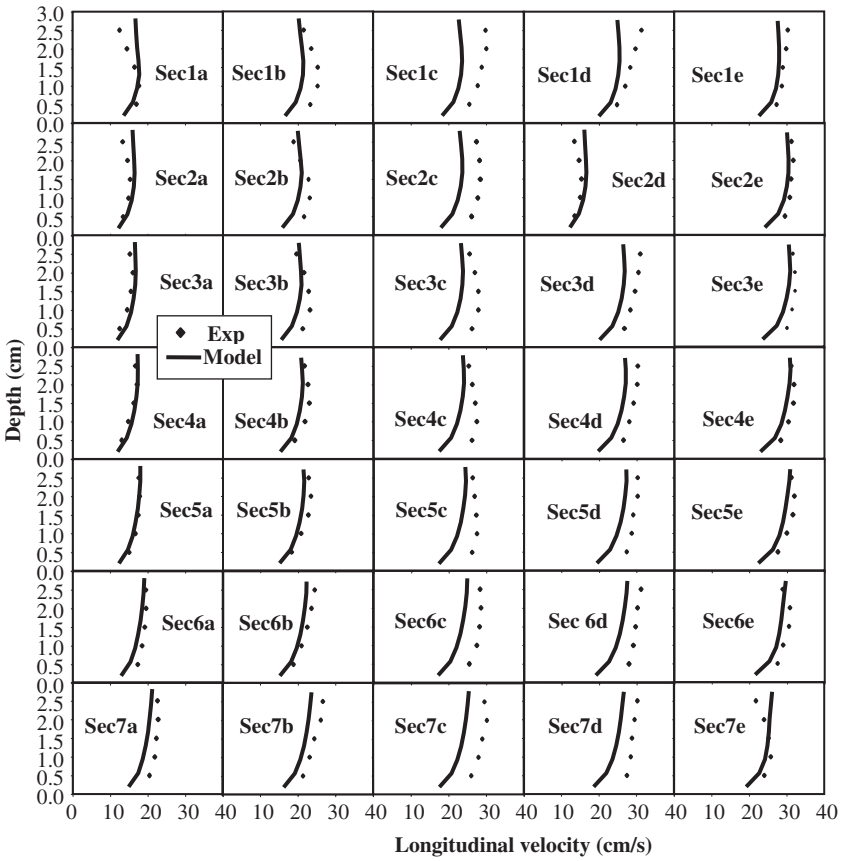

Figure 10. Longitudinal velocity profiles at different locations along the bend.

from the preceding bend and the development of an opposite secondary current in a present bend, as predicted by the model, are presented in Figure 11. As illustrated in Figure 11, at the beginning of the bend a secondary current exists and its direction is based on the preceding bend. It is apparent that further into the bend (see section 3) an opposite spiral flow forms near the bed. At the mid-bend section two opposite spiral flows can be seen. From the mid section to the end of the bend, the secondary current developed in the bend becomes stronger and near the end of the bend it occupies the whole section. The predictions of the flow characteristics made with the use this model are therefore in good agreement with the observations [23].

SUMMARY AND CONCLUSIONS

3-D shallow water equations are generally sufficient to describe the flow nature in rivers and open channels. A multi-layer model is developed in this study to solve these equations. In

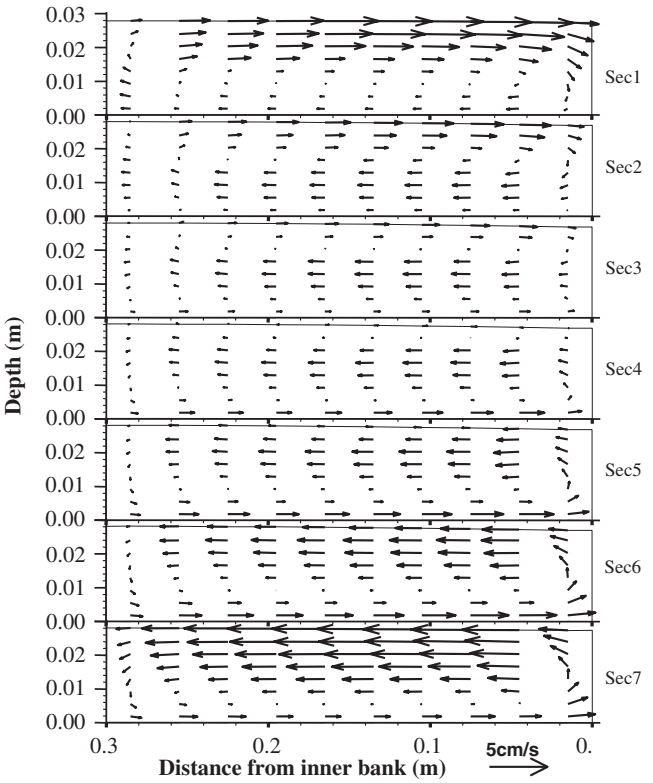

Figure 11. Simulated secondary flow pattern at different sections along the bend.

this model, the flow depth is divided into a number of layers and the shallow water equations are integrated in each layer to derive the governing equations. To deal with the irregular flow boundaries, a curvilinear co-ordinate system is employed. Large variations in flow depth and bed topography may exist in long channels. To locate the layers easily, it is assumed that each layer is non-horizontal with varying thickness in the flow domain.

Due to the similarity in governing equations, any 2-D depth averaged program can be upgraded to a 3-D multi-layer model. Such a development for a depth averaged model and its numerical scheme is described in this paper.

The model was verified for three different cases of open channel flow. In the first case, the water surface profile along a M2 profile was calculated and compared with the calculated results using the direct step method. The predicted velocity profiles in depth were also compared with the logarithmic distribution law. Both of these comparisons showed very good agreement.

Secondary circulation and free surface effects influence the developing region in a channel. In the second case, the predicted velocity distribution in depth in several sections along the centerline of a developing region was compared with experimental data. Despite the fact that a simple turbulent model was used, there was a good agreement between the experimental

and model results. This correlation demonstrates the ability of the model to carry out 3-D flow computations.

In the third case, secondary currents along a meandering channel were predicted using the model. The results of the simulation were then compared with experimental data. The mathematical model showed that at the beginning of a bend, a secondary current generated in the preceding bend occupied the whole section. Further downstream in the bend, the secondary flow generated in the present bend formed in an opposite direction near the flow bed. In the middle of the bend, two opposite spiral flows were observed in the section. Further downstream, the secondary current generated in the present bend became stronger and at the end of the bend it occupied the whole section. These calculations were in good agreement with observations. Comparison of the longitudinal and transverse velocity profiles at many sections along a bend showed reasonable agreement, confirming the ability of a multi-layer model to simulate 3-D flow behaviour. To achieve more accurate results in complicated flow problems such as the meandering channel and the developing flow region, more advanced turbulent models should be considered for use in future research work.

NOMENCLATURE

a	coefficients of discretized equations
B	width of the channel
C	constant of integration
F	mass flux
g	the gravitational acceleration
H	total depth
h_k	thickness of the kth layer
J	the Jacobian
k_s	absolute roughness
q_{ij}	metric tensor
p	pressure
u	Cartesian component of velocity in x direction
U	layer averaged component of velocity in x direction
U_c	contravariant layer averaged velocity components along ξ line
U_e	velocity at water surface
u_*	bed shear velocity
v	Cartesian component of velocity in y directions
V	layer averaged velocity components in y line
V_c	contravariant layer averaged velocity components along η line
w	velocity component in z directions
$x_\xi, x_\eta, y_\xi, y_\eta$	the metrics
z	distance along the z axis
$\Delta\eta, \Delta\xi$	dimensions of mesh in the computational domain
ϕ	U or V
κ	von Karman constant
ρ	density

υ_t	eddy viscosity
ζ	water surface elevation

Superscripts

$*$	value of quantity from previous iteration
$'$	quantity correction
U, V	related to momentum equations in the x and y directions, respectively

Subscripts

$k, k+1$	bottom and top surfaces of a layer along the z axis, respectively
P, E, W, N, S	grid point and four neighbouring points around it
e, w, n and s	positions at the face of the scalar cells
nb	neighbouring points

APPENDIX A. GOVERNING EQUATIONS IN CURVILINEAR CO-ORDINATE SYSTEM

Continuity:

$$\frac{\partial(U_c h_k)}{\partial \xi} + \frac{\partial(V_c h_k)}{\partial \eta} + M_c|_{z_k} - M_c|_{z_{k+1}} = 0 \tag{A1}$$

where

$$M_c = \left(U_c \frac{\partial z}{\partial \xi} + V_c \frac{\partial z}{\partial \eta} - Jw \right)$$

and U_c and V_c are Contravariant layer averaged velocity components along ξ and η lines; z is distance along the z axis, and J is the Jacobian.

Momentum:

$$\frac{\partial}{\partial \xi}(U_c h_k \phi) + \frac{\partial}{\partial \eta}(V_c h_k \phi) = \frac{\partial}{\partial \xi}\left\{ J \upsilon_t q_{11} \frac{\partial(\varphi h_k)}{\partial \xi} \right\} + \frac{\partial}{\partial \eta}\left\{ J \upsilon_t q_{22} \frac{\partial(\varphi h_k)}{\partial \eta} \right\} + JS^{\phi} + JS_c^{\varphi}|_{z_k} - JS_c^{\varphi}|_{z_{k+1}} \tag{A2}$$

where

$$S^U = -\frac{1}{J} g h_k \left\{ y_\eta \frac{\partial \zeta}{\partial \xi} - y_\xi \frac{\partial \zeta}{\partial \eta} \right\} + \frac{1}{J} \frac{\partial}{\partial \xi}\left\{ J \upsilon_t q_{12} \frac{\partial(U h_k)}{\partial \eta} \right\} + \frac{1}{J} \frac{\partial}{\partial \eta}\left\{ J \upsilon_t q_{21} \frac{\partial(U h_k)}{\partial \xi} \right\}$$

$$S^V = -\frac{1}{J} gh_k \left\{ -x_\eta \frac{\partial \zeta}{\partial \xi} + x_\xi \frac{\partial \zeta}{\partial \eta} \right\} + \frac{1}{J} \frac{\partial}{\partial \xi} \left\{ J \upsilon_t q_{12} \frac{\partial (V h_k)}{\partial \eta} \right\} + \frac{1}{J} \frac{\partial}{\partial \eta} \left\{ J \upsilon_t q_{21} \frac{\partial (V h_k)}{\partial \xi} \right\}$$

$$S_c^U = v_t \left\{ 2 \left(q_{11} \frac{\partial z}{\partial \xi} + q_{12} \frac{\partial z}{\partial \eta} \right) \frac{\partial u}{\partial \xi} + 2 \left(q_{21} \frac{\partial z}{\partial \xi} + q_{22} \frac{\partial z}{\partial \eta} \right) \frac{\partial u}{\partial \eta} - \frac{\partial u}{\partial z} \right\} - M_c \cdot u$$

$$S_c^V = v_t \left\{ 2 \left(q_{11} \frac{\partial z}{\partial \xi} + q_{12} \frac{\partial z}{\partial \eta} \right) \frac{\partial v}{\partial \xi} + 2 \left(q_{21} \frac{\partial z}{\partial \xi} + q_{22} \frac{\partial z}{\partial \eta} \right) \frac{\partial v}{\partial \eta} - \frac{\partial v}{\partial z} \right\} - M_c \cdot v$$

$$U_c = y_\eta U - x_\eta V$$

$$V_c = -y_\xi U + x_\xi V$$

$$q_{11} = \frac{1}{J^2}(y_\eta^2 + x_\eta^2), \quad q_{12} = q_{21} = -\frac{1}{J^2}(y_\eta y_\xi + x_\eta x_\xi), \quad q_{22} = \frac{1}{J^2}(y_\xi^2 + x_\xi^2)$$

In these equations ϕ is U or V, layer averaged components of velocity in x or y directions, respectively; υ_t is eddy viscosity; g is the gravitational acceleration; and x_ξ, x_η, y_ξ, and y_η are the metrics.

ACKNOWLEDGEMENTS

The authors would like to thank Dr. C. J. Lai for his advice and suggestions, and Prof. N. Tamai for providing experimental data of the meandering channel. The study was partially supported by the National Science and Engineering Research Council of Canada.

REFERENCES

1. Vreugdenhil CB. *Numerical Methods for Shallow Water Flows*. Kluwer Academic Publishers: Dordrecht, 1994.
2. Vreugdenhil CB, Wijbenga J. Computation of flow pattern in rivers. *Journal of Hydraulic Division* (ASCE) 1982; **108**(11):1296–1310.
3. Molls T, Chaudhry HM. Depth-averaged open channel model. *Journal of Hydraulic Engineering* (ASCE) 1995; **121**(6):453–465.
4. Jin YC, Steffler PM. Predicting flow in curved open channels by depth-averaged method. *Journal of Hydraulic Engineering* (ASCE) 1993; **119**(1):109–114.
5. Ye J, McCorquodale JA. Depth averaged hydrodynamic model in curvilinear collocated grid. *Journal of Hydraulic Engineering* (ASCE) 1997; **123**(5):380–388.
6. Wei OWH, Lu Q, Li YS. Multi-layer modeling of three-dimensional hydrodynamic transport processes. *Journal of Hydraulic Research* 1997; **34**(5):677–693.
7. Kodama T, Wang SSY, Kawahara M. Model verification on 3D tidal current analysis in Tokyo bay. *International Journal for Numerical Methods in Fluids* 1996; **22**:43–66.
8. Li YS, Zhan JM. An efficient three-dimensional semi-implicit finite element scheme for simulation of free surface flows. *International Journal for Numerical Methods in Fluids* 1993; **16**:187–198.
9. Kim CK, Li JS. A three-dimensional PC-based hydrodynamic model using an ADI scheme. *Coastal Engineering* 1994; **23**:271–287.
10. Reggio M, Hess A, Ilinca A. 3-D multiple-level simulation of free surface flows. *Journal of Hydraulic Research* 2002; **40**(4):413–423.
11. Li CW, Yu TS. Numerical investigation of turbulent shallow recirculating flows by a quasi-three-dimensional k-ε model. *International Journal for Numerical Methods in Fluids* 1996; **23**:485–501.
12. Lai CJ, Yen CW. Turbulent free surface flow simulation using a multi-layer model. *International Journal for Numerical Methods in Fluids* 1993; **16**:1007–1025.
13. Shankar NJ, Chan ES, Zhang QY. Three-dimensional numerical simulation for an open channel flow with a constriction. *Journal of Hydraulic Research* 2001; **39**(2):187–201.

14. Patankar SV. *Numerical Heat Transfer and Fluid Flow*. Hemisphere Publishers: Washington, DC, 1980.
15. Weerakoon SB, Tamai N, Kawahara Y. A depth correction equation for depth-averaged flow computations in natural rivers. *Proceedings of the Environmental Hydraulics Conference*, Hong Kong, 1991.
16. Zhou JG. Velocity-depth coupling in shallow water flows. *Journal of Hydraulic Engineering* (ASCE) 1995; **121**(10):717–724.
17. Shyy W, Tong SS, Correa SM. Numerical recirculating flow calculation using a boundary-fitted coordinate system. *Numerical Heat Transfer* 1985; **8**:99–113.
18. Launder BE, Spalding DB. The numerical calculation of turbulent flows. *Computer Methods in Applied Mechanics and Engineering* 1974; **3**:264–287.
19. Chow VT. *Open Channel Hydraulics*. McGraw-Hill: New York, 1959.
20. Schlichting H. *Boundary Layer Theory* (6th edn). McGraw-Hill: New York, 1968.
21. Ranga Raju KG, Asawa GL, Mishra HK. Flow-establishment length in rectangular channels and ducts. *Journal of Hydraulic Engineering* (ASCE) 2000; **126**(7):533–539.
22. Nezu I, Rodi W. Open channel flow measurements with a laser Doppler anemometer. *Journal of Hydraulic Engineering* (ASCE) 1986; **112**(5):335–355.
23. Tamai N, Ikeuchi K, Yamazaki A, Mohamed AA. Experimental analysis on the open channel flow in rectangular continuous bends. *Journal of Hydroscience and Hydraulic Engineering* 1983; **1**(2):17–31.

